MOS-like approach for compact modeling of High-Electron-Mobility Transistor

Adrien Vaysset
CEA, LETI, Univ. Grenoble Alpes,
38000 Grenoble, France
adrien.vaysset@cea.fr

Sébastien Martinie
CEA, LETI, Univ. Grenoble Alpes,
38000 Grenoble, France
sebastien.martinie@cea.fr

François Triozon
CEA, LETI, Univ. Grenoble Alpes,
38000 Grenoble, France
francois.triozon@cea.fr

Olivier Rozeau
CEA, LETI, Univ. Grenoble Alpes,
38000 Grenoble, France
olivier.rozeau@cea.fr

Marie-Anne Jaud
CEA, LETI, Univ. Grenoble Alpes,
38000 Grenoble, France
marie-anne.jaud@cea.fr

René Escoffier
CEA, LETI, Univ. Grenoble Alpes,
38000 Grenoble, France
rene.escoffier@cea.fr

Thierry Poiroux
CEA, LETI, Univ. Grenoble Alpes,
38000 Grenoble, France
thierry.poiroux@cea.fr

***Abstract*—High-Electron-Mobility Transistor (HEMT) with AlGaN/GaN gate stack is a promising candidate for high-speed and high-power applications. Recent HEMT compact modeling works have proposed threshold-based [1] and surface-potential-based models [2]. In the latter approach, inversion charge is calculated from the quantum expression of a 2-dimensional electron gas (2DEG). Here, we investigate the possibility to model HEMTs with a MOSFET-like approach whereby quantum confinement is included as an effective bandgap widening in the surface potential equation. We evidence that such a MOSFET-like approach leads to a more accurate description over the whole polarization range, especially in the moderate inversion regime. This analytical model is validated by Poisson-Schrödinger numerical simulations. Furthermore, to address a specific feature of HEMT devices, a field plate model is also presented.**

***Index Terms*—Power device, GaN, HEMT, compact model, SPICE**

I. Surface potential calculation: quantum confinement correction

In the surface-potential-based ASM-HEMT model [3], the HEMT channel is modeled as a 2DEG. Its quantum expression is directly included in the surface potential equation, assuming charge sheet approximation with 2D degeneracy and Fermi-Dirac statistics [4]. The complexity of this model contrasts with the usual approach of MOS compact models that build upon classical physics and include quantum effects as a correction.

Here, we propose an approach similar to MOS models to describe HEMT devices. First, the Poisson equation is solved classically, using Boltzmann statistics. Then, quantum confinement is added as an effective bandgap widening through triangular-well approximation [5]. The resulting surface potential equation is similar to the one used in MOS compact models. Therefore, current, charge and other features can be readily implemented with proven methods.

The device studied here is shown in Fig. 1. Firstly, to derive the surface potential Ψ_s, we consider only the AlGaN/GaN stack.

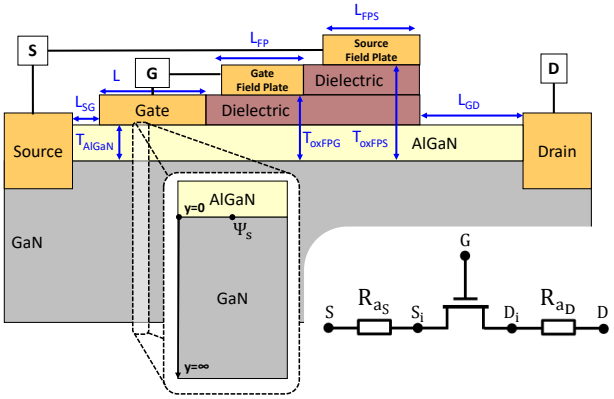

Fig. 1. HEMT structure definition for n-type configuration including Gate and Source field plate description. Inset shows the equivalent circuit in-cluding non-linear resistance (Si and Di are internal nodes).

Considering only the inversion charge and no GaN doping, the Poisson equation is derived in the classical case.

$$\frac{d^2x}{dy^2} = \frac{1}{\Phi_T\,\epsilon_{GaN}\,q\,n_i\exp\left(x - x_n\right)} \tag{1}$$

where Φ_T is the thermal voltage, $x = \Psi/\Phi_T$ is the normalized potential, y is the vertical coordinate, ϵ_{GaN} is the GaN permittivity, q is the electron charge, n_i is the intrinsic concentration and $x_n = V_D/\Phi_T$ is the normalized quasi-Fermi level.

The research leading to these results has received funding from the collaborative research program between CEA-Leti and SILVACO.

Then, using the boundary conditions

$$\frac{dx}{dy}(y=0) = \frac{C_{AlGaN}}{\epsilon_{GaN}(x_g - x)} \tag{2}$$

$$\frac{dx}{dy}(y \to \infty) = 0\ , \tag{3}$$

the implicit surface potential equation is obtained:

$$(x_g - x_s)^2 = G^2 \exp(x_s - x_n). \tag{4}$$

Then, following the same approach as [5], an energy shift is introduced to account for quantum effects,

$$(x_g - x_s)^2 = G^2 \exp\left(x_s - x_n - K_Q\,(x_g - x_s)^{2/3}\right) \tag{5}$$

$G^2 = 2qn_i\epsilon_{GaN}/C_{AlGaN}^2\Phi_T$, K_Q is the quantum parameter and C_{AlGaN} is the AlGaN capacitance. The shift $-K_Q\,(x_g - x_s)^{2/3}$ corresponds to the difference between the bottom of the "classical" conduction band and the first occupied sub-band, assuming a triangular energy well. The limitations of this approximation have been discussed extensively [6]. According to the consensus, this is sufficient to capture the global behavior of the quantum effect, particularly in moderate inversion. For strong inversion, accuracy decreases due to non-consideration of Fermi-Dirac statistics. However, fitting can still be improved by slightly tuning the related charge parameters.

The numerical solution of (4) and (5) is plotted in Fig. 2(a).

The exact solution of (4) is expressed via the Lambert $\mathcal{W}_0$ function.

$$x_{s,0} = x_g - 2\ \mathcal{W}_0\left(\frac{G}{2}\exp\left(\frac{x_g}{2}\right)\right) \tag{6}$$

An analytical approximation of the $\mathcal{W}_0$ function exists.

$$\mathcal{W}_0(x) \sim \ln(1+x)\left(1 - \frac{\ln(1+\ln(1+x))}{2+\ln(1+x)}\right) \tag{7}$$

It can be used as an initial guess in the implicit surface potential equation (4). Then, an error correction based on a 2nd-order Taylor expansion is applied twice.

$$x_{s,1} = x_{s,0} + e_2(x_{s,0}) \tag{8}$$

$$x_{s,2} = x_{s,1} + e_2(x_{s,1}) \tag{9}$$

where the function $e_2(x)$ is defined as

$$e_2(x) = \frac{a(x)}{b(x) + \frac{a(x)\,c(x)}{b(x)}}(x_g - x). \tag{10}$$

and the functions $a(x)$, $b(x)$ and $c(x)$ are defined as

$$a(x) = \ln(x_g - x) - \ln(G) - \frac{x}{2} + \frac{K_Q}{2}(x_g - x)^{2/3} \tag{11}$$

$$b(x) = 1 + \frac{1}{2}(x_g - x) + \frac{K_Q}{3}(x_g - x)^{2/3} \tag{12}$$

$$c(x) = \frac{1}{2} + \frac{K_Q}{18}(x_g - x)^{2/3} \tag{13}$$

The error is brought below the numerical noise, as shown in Fig. 2(b,c).

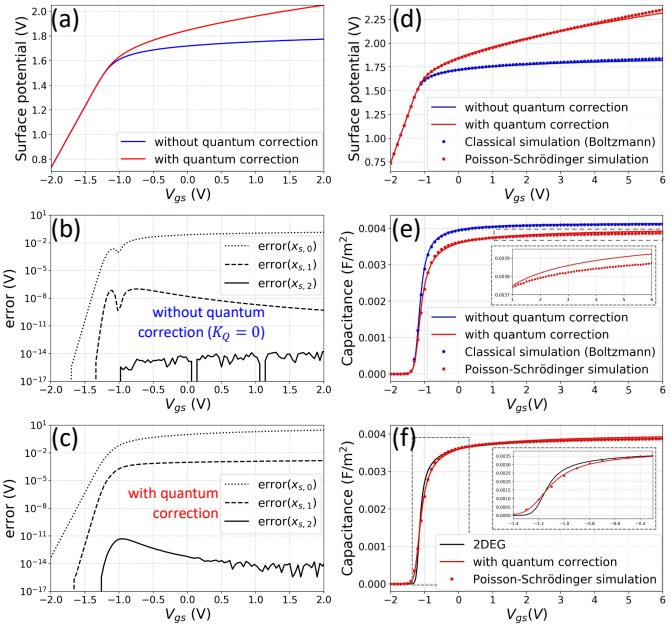

Fig. 2. (a) Surface potential as a function of gate voltage in the case of (4) (without quantum correction) and (5) (with quantum correction); (b,c) Absolute error of the initial guess $x_{(s,0)}$ and the explicit solutions $x_{(s,1)}$ and $x_{(s,2)}$ of (8) and (8). Surface potential (d) and associated capacitance (e) for model (solid lines) and simulations (dots). (f) Comparison with the 2DEG model with inset in the moderate inversion regime.

To validate our model, we have developed a dedicated Poisson-Schrödinger numerical solver for AlGaN/GaN stack. Figs. 2(d,e) illustrate the comparison between the Poisson-Schrödinger solver and the model. It also includes numerical simulations with Boltzmann statistics. The full model from (5) and the classical model from (4) are in good agreement with the Poisson-Schrödinger solver and the Boltzmann simulations, respectively.

For a complete comparison, in Fig. 2(f), the capacitance is also plotted for an analytical 2DEG model. This model is obtained with charge sheet approximation and Fermi-Dirac statistics in a 2-dimensional electron gas, considering only the first energy level. It obeys the following equation:

$$x_g - x_s = \alpha\,\ln\left(1 + \exp\left(x'_s - K_Q(x_g - x_s)^{2/3}\right)\right) \tag{14}$$

where $\alpha = \frac{qd}{\epsilon_{AlGaN}}\frac{m_e kT}{\pi\hbar^2\Phi_T}$ (where d is the AlGaN layer thickness) and $x'_s = x_s + \frac{E_c - E_g/2}{q\Phi_T}$ (where E_c is the bottom of the energy well).

In moderate inversion, our MOS-like model is in good agreement with the Poisson-Schrödinger solution, while the 2DEG model exhibits a more abrupt transition (inset of Fig. 2f). Since the energy well is shallow in moderate inversion, it is similar to an energy continuum. Therefore, it is better described by the MOS-like model based on classical physics. In strong inversion, the 2DEG model is more accurate than the MOS-like model. This is due to greater confinement. However, this discrepancy can be compensated by slightly tuning the effective AlGaN layer thickness, as already mentioned.

Finally, one of the main advantages of the proposed model is its simplicity in terms of implementation. Moreover, it builds upon previous MOS models, which means that implementation of current, charge and other features can be done in a similar way.

II. Current and charge calculation including field plates

Implementation of the current is similar to the Leti-NSP model [7]. The main features have been adapted from this model, such as mobility degradation (including Coulomb scattering, phonon and surface roughness), saturation velocity, channel length modulation and self-heating effect. One of the main differences is the description of source/drain access resistance and the addition of field plates. Access resistance was modeled similarly to previous work [8], thus adding an internal node and an extra resistance with nonlinear current dependence [9], as illustrated in the inset of Fig. 1.

$$R_{a_{S,D}} = R_{L_{S,D}} + \frac{R_{NL_{S,D}}}{\left(1 - \left(\frac{I_{ds}}{\mathrm{ISAT_{S,D}}}\right)^{\beta_{S,D}}\right)^{1/\beta_{S,D}}} \tag{15}$$

where $R_{L_{S,D}}$, $R_{NL_{S,D}}$, $\mathrm{ISAT_{S,D}}$ and $\beta_{S,D}$ are the nonlinear access parameters and I_{ds} is the drain current. Fig. 3 illustrates the model versus experimental data from [9].

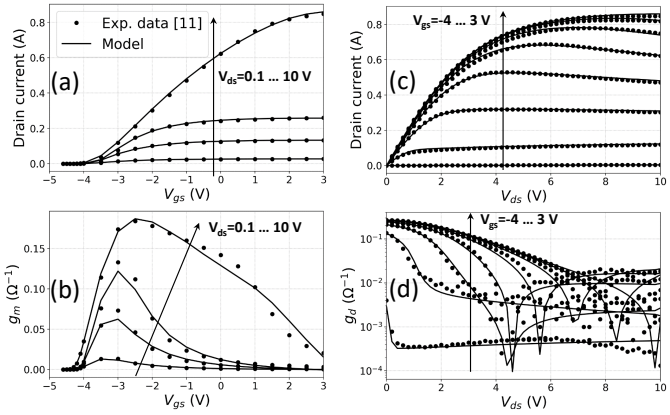

Fig. 3. Comparison between experimental data from reference [9] and model for I_d vs V_{gs} (a), $g_m = dI_d/dV_{gs}$ vs V_{gs} (b), I_d vs V_{ds} (c) and $g_d = dI_d/dV_{ds}$ vs V_{ds} (d). Dots show experimental data. Solid lines represent the model.

Field plate modeling is challenging. Former work [10] uses duplication of internal node to capture each field plate effect. Here, we propose to add only a parasitic field plate charge without adding any internal node, in the same way a parasitic charge is induced by an overlap capacitance [11]. In practice, the charge calculation reuses the surface potential procedure with dedicated parameters for field plate workfunction, interface state and geometry. In HEMT, the field plate dielectric thickness is larger than the field plate length. Therefore, the dependence of field plate charge with longitudinal field is neglected. Equations (16) and (17) express gate and source field plate charges.

$$Q_{FP_G} = C_{ox,FP_G}\left(x_{g,FP_G} - x_{s,FP_G}\right) \tag{16}$$

where C_{ox,FP_G} is the gate field plate dielectric capacitance, $x_{g,FP_G} = \frac{V_{GD} - V_{off,FP_G}}{\Phi_T}$ and V_{off,FP_G} is the cut-off voltage of the gate field-plate.

$$Q_{FP_S} = C_{ox,FP_S}\left(x_{g,FP_S} - x_{s,FP_S}\right) \tag{17}$$

where C_{ox,FP_S} is the source field plate dielectric capacitance, $x_{g,FP_S} = \frac{V_{SD} - V_{off,FP_S}}{\Phi_T}$ and V_{off,FP_S} is the cut-off voltage of the source field-plate.

Fig. 4 illustrates model versus experimental data from reference [10]. Note that drain and depletion capacitances are added in order to capture C_{oss} (or C_{sd}) capacitance.

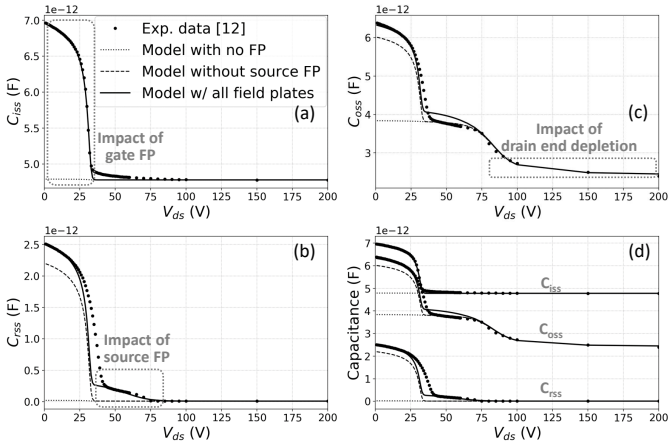

Fig. 4. Comparison between experimental data from reference [10] and model for C_{iss} (a), C_{rss} (b), C_{oss} (c) and these three capacitances (d). Dots are for experimental data; solid line is for the model including all the field plates (FP); dashed line is the model without source FP; dotted line is the model without any FP.

III. Conclusion

We have developped a surface-potential-based compact model for HEMT devices. Similarly to MOS models, quantum confinement is described as a simple energy shift, corresponding to the difference between the bottom of the "classical" conduction band and the first occupied sub-band. Above this first energy level, the conduction band is treated as a continuum, using Boltzmann statistics. Thankfully, a good initial guess exists for the entire polarization range. Applying a Taylor-based error correction, the accuracy can go beyond numerical precision. Our model matches very well Poisson-Schrödinger simulations in the moderate inversion regime. In strong inversion, the slight difference can be compensated with fitting parameters. One main advantage of the model, beside its simplicity, is its close resemblance to other surface-potential-based MOS models such as PSP. This means that charge, current and other features can be readily implemented with proven methods.

Finally, we have adressed a specific feature of HEMT devices: the field plates. In order to minimize the number of fitting parameters and avoid additional internal nodes, field plate charge is added similarly to a parasitic charge induced by an overlap resistance. Capacitance and currents are fitted on experimental data, demonstrating model capability in a real case.

ACKNOWLEDGMENT

The authors thank Bogdan Tudor and Eric Guichard from SILVACO for fruitful discussions and collaboration.

REFERENCES

[1] MVSG model. [Online]. Available: https://uwaterloo.ca/waterloo-emerging-integrated-systems-group/mvsg-model
[2] ASM-HEMT model. [Online]. Available: http://iitk.ac.in/asm/
[3] S. Khandelwal, Y. S. Chauhan, T. A. Fjeldly, S. Ghosh, A. Pampori, D. Mahajan, R. Dangi, and S. A. Ahsan, "Asm gan: Industry standard model for gan rf and power devices—part 1: Dc, cv, and rf model," *IEEE Transactions on Electron Devices*, vol. 66, no. 1, pp. 80–86, 2019.
[4] S. Kola, J. M. Golio, and G. N. Maracas, "An analytical expression for fermi level versus sheet carrier concentration for hemt modeling," *IEEE Electron Device Letters*, vol. 9, no. 3, pp. 136–138, 1988.
[5] G. Gildenblat, T. L. Chen, and P. Bendix, "Closed-form approximation for the perturbation of MOSFET surface potential by quantum-mechanical effects," *Electronics Letters*, vol. 36, no. 12, pp. 1072–1073, 2000.
[6] R. van Langevelde, A. Scholten, and D. Klaassen. MOS Model 11. [Online]. Available: https://www.nxp.com/wcm_documents/models/mos-models/model-11/nltn2004_00085.pdf
[7] O. Rozeau, S. Martinie, T. Poiroux, F. Triozon, S. Barraud, J. Lacord, Y. M. Niquet, C. Tabone, R. Coquand, E. Augendre, M. Vinet, O. Faynot, and J. . Barbé, "NSP: Physical compact model for stacked-planar and vertical gate-all-around mosfets," in *2016 IEEE International Electron Devices Meeting (IEDM)*, 2016, pp. 7.5.1–7.5.4.
[8] D. R. Greenberg and J. A. del Alamo, "Velocity saturation in the extrinsic device: a fundamental limit in HFET's," *IEEE Transactions on Electron Devices*, vol. 41, no. 8, pp. 1334–1339, 1994.
[9] S. Ghosh, S. A. Ahsan, Y. S. Chauhan, and S. Khandelwal, "Modeling of source/drain access resistances and their temperature dependence in GaN HEMTs," in *2016 IEEE International Conference on Electron Devices and Solid-State Circuits (EDSSC)*, 2016, pp. 247–250.
[10] S. Aamir Ahsan, S. Ghosh, K. Sharma, A. Dasgupta, S. Khandelwal, and Y. S. Chauhan, "Capacitance modeling in dual field-plate power GaN HEMT for accurate switching behavior," *IEEE Transactions on Electron Devices*, vol. 63, no. 2, pp. 565–572, 2016.
[11] PSP model. [Online]. Available: http://www.cea.fr/cea-tech/leti/pspsupport